Chemistry and Physics of Lipids 213 (2018) 102–110

Contents lists available at ScienceDirect

Chemistry and Physics of Lipids

journal homepage: www.elsevier.com/locate/chemphyslip

Phase behavior of palmitoyl and egg sphingomyelin

Zoran Arsov[a,1], Emilio J. González-Ramírez[b,1], Felix M. Goñi[b], Stephanie Tristram-Nagle[c], John F. Nagle[c,*]

[a] Department of Condensed Matter Physics, Laboratory of Biophysics, Jozef Stefan Institute, 1000 Ljubljana, Slovenia
[b] Instituto Biofísika (CSIC, UPV/EHU) and Departamento de Bioquímica, Universidad del País Vasco, 48080 Bilbao, Spain
[c] Physics Department, Carnegie Mellon University, Pittsburgh, PA 15213, United States

ARTICLE INFO

Keywords:
X-ray diffraction
X-ray diffuse scattering
Volume determination
Ripple phase
Gel phase
Fluid phase
Ripple wavelength

ABSTRACT

Despite the biological significance of sphingomyelins (SMs), there is far less structural information available for SMs compared to glycerophospholipids. Considerable confusion exists in the literature regarding even the phase behavior of SM bilayers. This work studies both palmitoyl (PSM) and egg sphingomyelin (ESM) in the temperature regime from 3 °C to 55 °C using X-ray diffraction and X-ray diffuse scattering on hydrated, oriented thick bilayer stacks. We observe clear evidence for a ripple phase for ESM in a large temperature range from 3 °C to the main phase transition temperature (T_M) of ~38 °C. This unusual stability of the ripple phase was not observed for PSM, which was in a gel phase at 3 °C, with a gel-to-ripple transition at ~24 °C and a ripple-to-fluid transition at ~41 °C. We also report structural results for all phases. In the gel phase at 3 °C, PSM has chains tilted by ~30° with an area/lipid ~45 Å^2 as determined by wide angle X-ray scattering. The ripple phases for both PSM and ESM have temperature dependent ripple wavelengths that are ~145 Å near 30 °C. In the fluid phase, our electron density profiles combined with volume measurements allow calculation of area/lipid to be ~64 Å^2 for both PSM and ESM, which is larger than that from most of the previous molecular dynamics simulations and experimental studies. Our study demonstrates that oriented lipid films are particularly well-suited to characterize ripple phases since the scattering pattern is much better resolved than in unoriented samples.

1. Introduction

The major lipids in biological membranes are glycerophospholipids, sphingolipids and sterols. While sphingolipids include glycosphingolipids and sphingomyelins (SMs), the latter are the most abundant sphingolipids in mammalian cells (van Meer et al., 2008) reaching concentrations of 15% of the total phospholipid content in the outer leaflet of the plasma membranes (Shaw et al., 2012). Structurally, SMs are similar to phosphatidylcholines (PCs) in that both lipids have phosphatidylcholine as the polar headgroup and both have long hydrocarbon tails, but there are considerable differences in the linkages between these parts of the lipids (Ramstedt and Slotte, 2002).

Recent interest in SMs arises from their interaction with cholesterol in generating cholesterol-rich lateral membrane domains, their specific binding to and regulation of particular membrane proteins, and their involvement as precursors to simpler sphingolipids in cell signaling events (Goni and Alonso, 2006; Slotte, 2013). The preferential mixing of sterols with SMs over PCs is mainly attributed to two properties: Firstly, SMs usually have saturated or *trans*-unsaturated tails and they apparently pack more tightly (van Meer et al., 2008); secondly, the amide and hydroxyl groups in SMs can act as hydrogen bond donors and acceptors, so they can form both intra- and intermolecular hydrogen bonding (Slotte, 2016; Venable et al., 2014).

Since pure SMs are more expensive than pure PCs, many experimental studies of systems involving them are performed using natural SM extracts e.g., egg, brain and milk SMs, which have mixtures of hydrocarbon chains. On the other hand, simulation studies use pure SM lipids with homogeneous chains. Egg SM (ESM) stands out as the most homogeneous of the natural SMs; it has predominantly 86% N-palmitoyl (16:0) acyl chain (Filippov et al., 2006) with 93% of the sphingosine (18:1) long-chain base (Ramstedt et al., 1999). Therefore from the viewpoint of composition, ESM is the closest natural extract to the pure palmitoyl sphingomyelin (PSM), so experimental properties using ESM are frequently compared to simulation studies using PSM (Niemela et al., 2004); such comparisons should be made carefully, especially as the main transition temperature of PSM (T_M = 41 °C) (Barenholz et al., 1976) is somewhat higher than for ESM (T_M = 38 °C) (Jimenez-Rojo et al., 2014). This paper will further address differences between ESM

* Corresponding author.
E-mail address: nagle@cmu.edu (J.F. Nagle).
[1] Contributed equally as first co-authors.

https://doi.org/10.1016/j.chemphyslip.2018.03.003
Received 14 December 2017; Received in revised form 2 February 2018; Accepted 6 March 2018
Available online 22 April 2018

and PSM.

Even the nature of the generic SM main transition has been unclear. By analogy with saturated PC lipids, the transition is often inferred to be from ripple phase to fluid (liquid-crystalline or liquid-disordered) phase if a pretransition is observed and gel-to-fluid phase if it is not. Many thermotropic studies did not observe a pretransition, either in PSM (de Almeida et al., 2003; Maulik and Shipley, 1996), or in ESM (Anderle and Mendelsohn, 1986; Arsov and Quaroni, 2008; Chien et al., 1991; Epand and Epand, 1980; Garcia-Arribas et al., 2016; Jimenez-Rojo et al., 2014; Mannock et al., 2003; Mckeone et al., 1986; Rujanavech et al., 1986; Steinbauer et al., 2003; Veiga et al., 2001), and have described the transition as from a gel-to-fluid (liquid-crystalline or liquid-disordered) phase.

Other PSM studies (Barenholz et al., 1976; Calhoun and Shipley, 1979) observed a pretransition using DSC. Turning to structural studies one of the first low- and wide-angle X-ray scattering (LAXS and WAXS) studies on PSM reported a gel phase structure below T_M despite observing a pretransition using DSC (Calhoun and Shipley, 1979). (Maulik and Shipley, 1996) also reported no X-ray evidence for a ripple phase in PSM. However, other X-ray studies have reported that ESM is in a ripple phase below T_M (Chemin et al., 2008; Quinn and Wolf, 2009; Shaw et al., 2012). All of these X-ray studies employed unoriented MLV samples where ripple reflections are either small or weak. By contrast, X-ray diffraction from oriented lipid samples is particularly well suited to differentiate between flat gel or interdigitated phases and the ripple phase (Akabori and Nagle, 2015; Guler et al., 2009; Katsaras et al., 2000; Sun et al., 1996b). To clarify the above mentioned differences in the literature for both ESM and PSM individually, as well as what the actual differences are between ESM and PSM, the aim of this work is to characterize the structure of the phases, particularly for $T < T_M$, using oriented hydrated samples.

A broad temperature interval was investigated and our results show that ESM persists in a ripple phase at all studied temperatures below T_M (3–35 °C), i.e., no gel phase or gel-to-ripple phase pretransition was observed. This persistence enabled us to study the temperature dependence of the ESM ripple phase structural parameters. In contrast, we find that PSM is in a gel phase below 24 °C and in a ripple phase between 24 °C and the main transition. Our study confirms that it is particularly valuable to study oriented lipid films, especially for ripple phases, since their scattering patterns are much better resolved than in unoriented MLV samples. It will also serve to alleviate a relative dearth in structural studies of PSM and ESM.

2. Materials & methods

2.1. Reagents & lipids

Egg sphingomyelin (ESM) (Lot Egg-SM 860061-01-115) and palmitoyl sphingomyelin (PSM) (Lot 860584-01-017) were purchased from Avanti Polar Lipids (Alabaster, AL) and used as received. Avanti estimates 1–1.5% L-erythro impurity, no D- or L-threo impurity, and greater than 99% purity with respect to total sphingomyelin content in PSM, whereas as much as 10% L-threo may occur when synthesizing by hydrolysis of natural SM. HPLC organic solvents were purchased from Sigma/Aldrich (St. Louis, MO).

2.2. Sample preparation

2.2.1. Oriented samples

4 mg of lyophilized lipid was dissolved in 200 mL chloroform:TFE (1:1) (v/v) and plated onto a silicon wafer (15 × 30 × 1 mm) via the rock and roll method (Tristram-Nagle, 2007) to produce stacks of ~1800 aligned bilayers (Tristram-Nagle et al., 2002). Solvents were removed by evaporation in a fume hood, followed by 2 h under vacuum at room temperature. The oriented samples were prehydrated at close to 100% RH in a polypropylene hydration chamber at 60 °C for 2 h and allowed to slowly cool to room temperature. Thin layer chromatography indicated no degradation due to this annealing procedure. Approximately 10 μm thick samples were trimmed to leave 5 mm (in the direction of the X-ray beam) by 30 mm (to provide many locations for the ~1 mm wide beam to minimize radiation damage).

2.2.2. Unoriented samples

2–10 mg of lyophilized lipid was mixed with 100 μL of MilliQ water. Samples were hydrated by vortexing and temperature cycling 3 times between 60 °C and 0 °C to form multilamellar vesicles (MLVs). Hydrated lipids were mildly centrifuged using a desk-top centrifuge in a glass test tube at 1000 rpm for 10 min and the concentrated lipid was loaded into 1 mm diameter thin-walled X-ray capillaries (Charles Supper Company, Natick, MA) and flame-sealed. The X-ray capillaries were centrifuged in a capillary holder at 1000 rpm for an additional 2 min to further concentrate the lipid in the beam. The final ratio of water to lipid was at least 2:1 so the MLVs were fully hydrated as evidenced by their contact with excess water in the capillary.

2.2.3. Volumetric samples

48.9 mg lyophilized ESM was added to 1.204 g MilliQ water and hydrated by vortexing and cycling three times between 60 and 0 °C. ~10 mg lyophilized PSM was added to ~1.1 g MilliQ water and hydrated by vortexing and cycling three times between 60 and 0 °C.

2.3. Methods

2.3.1. X-ray scattering

Oriented stacks of membrane mimics were hydrated through the vapor phase in a temperature-controlled hydration chamber described in (Kučerka et al., 2005). Low angle X-ray scattering (LAXS) and wide angle X-ray scattering (WAXS) were obtained from a Rigaku RUH3R rotating anode as described in (Tristram-Nagle et al., 2002; Tristram-Nagle et al., 1993). Wavelength was 1.5418 Å, and sample-to-detector (*S*)-distance was 280.6 mm (LAXS) and 133.7 mm (WAXS). Data were collected using a Rigaku (The Woodlands, TX) Mercury CCD array detector (1024 × 1024, 68 μm pixels) during 5- or 10 min dezingered scans. Temperature was controlled using a Julabo Model F25 circulating water bath. Data analysis for the ripple phase was performed as in (Sun et al., 1996b; Akabori and Nagle, 2015) using our proprietary TiffView software.

2.3.2. Volume measurements

The 4.1% aqueous ESM or ~1% aqueous PSM suspension was loaded into the Anton-Paar 5000 M DMA scanning density meter and heated at 12°/h.

3. Results

Fig. 1A shows the typical X-ray pattern obtained for ESM. Oriented samples clearly show off-specular peaks below T_M, indicated by white arrows; such peaks are required for in-plane periodicity that occurs for the ripple phase. The peaks are arranged symmetrically around the meridian because the sample is a powder average, in-plane only. This rippled pattern was present at every temperature investigated in this work from 3 to 35 °C. Additional oriented ESM data are shown in the Supplementary material (Figs. S1–S8). Following the literature (Akabori and Nagle, 2015; Sun et al., 1996b; Wack and Webb, 1989) these peaks can be indexed as (h,k) where the (h,0) peaks are the usual lamellar peaks that occur on the meridian with $q_r = 0$. The ripple side peaks are labeled with the k index. In Fig. 1A, the visible side peaks are, from the top, $(4,-2)$, $(3,-1)$, $(3,-2)$, $(2,-1)$, $(1,-1)$ and a weak (1,1). Fig. 1B shows that ESM is also in the ripple phase at 35 °C.

Fig. 2 shows LAXS data for PSM. At 37 °C (Fig. 2B) PSM is clearly in the ripple phase, however, at 3 °C (Fig. 2A) the absence of side peaks is consistent with a gel phase. In Fig. 2A, arcs, instead of spots, are due to

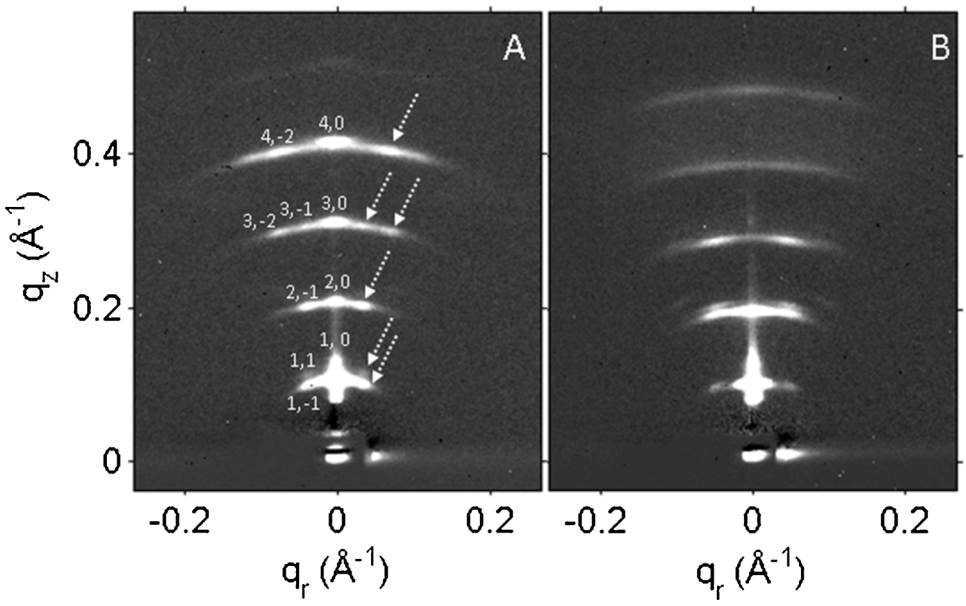

Fig. 1. LAXS data from oriented ESM. A. Overnight equilibration at 3 °C, followed by B. equilibration at 35 °C. White arrows in A. point to the off-specular peaks. D-spacing in A. is 60.3 Å and in B. is 65.8 Å.

mosaicity (Nagle et al., 2016). Additional oriented PSM data are shown in the Supplementary material (Figs. S9–S15).

In order to describe our structural results, a diagram of some of the basic structural parameters of ripple phases is shown in Fig. 3. The usual lamellar D-spacing in the z direction perpendicular to the substrate and the stack of bilayers includes the average bilayer thickness and the water spacing; it was obtained from the q_z positions of the specular (h,0) peaks. Following previous studies (Akabori and Nagle, 2015; Sun et al., 1996b; Wack and Webb, 1989), the in-plane spacing λ_r is the length of the rippled repeat distance; it was obtained from the q_r positions of the off-specular (h,k) peaks. γ is the angle in the two dimensional unit cell; it was obtained from the angle of the lines joining the central (h,0) peaks to the (h,k $<$ 0) side peaks (Akabori and Nagle, 2015; Sun et al., 1996b).

Fig. 4 shows results for λ_r and γ. The result that γ values differ from 90° requires that the ripple be asymmetric unlike the symmetric ripple phases that occur metastably in DPPC and which have λ_r greater than 200 Å (Katsaras et al., 2000; Mason et al., 1999; Rappolt and Rapp,

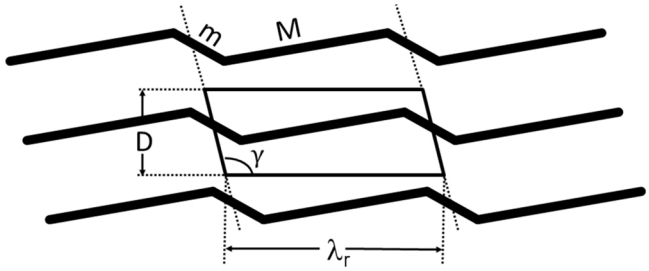

Fig. 3. Diagram of structural parameters characterizing the ripple phase. The bold solid lines represent the centers of three adjacent bilayers. M represents the major arm and m the minor arm in a typical saw-toothed asymmetric ripple (Akabori and Nagle, 2015; Katsaras et al., 2000; Sun et al., 1996b). D is the usual lamellar repeat D-spacing, λ_r is the ripple wavelength and γ the ripple offset angle in the unit cell indicated by the parallelogram containing the middle of the 2nd bilayer.

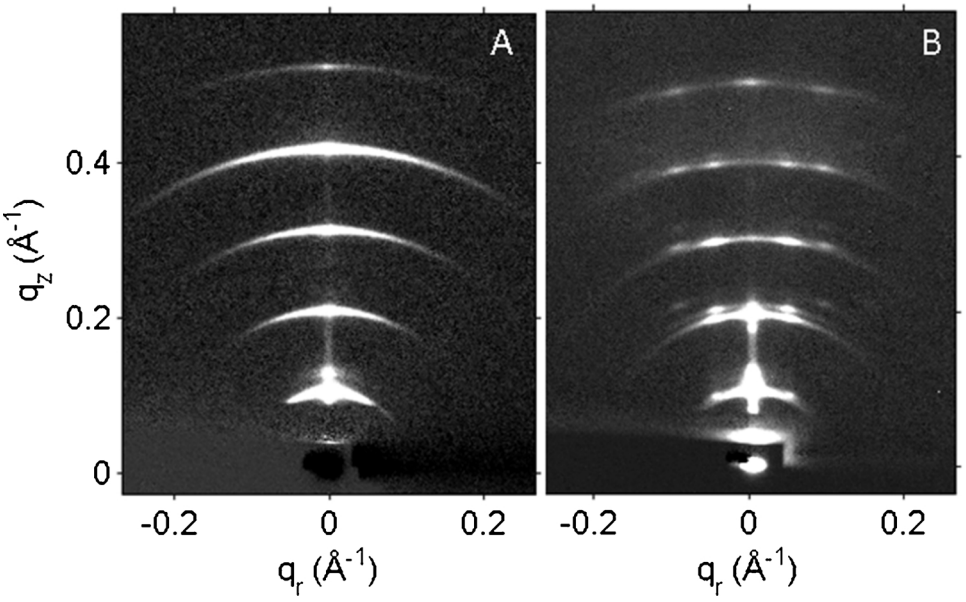

Fig. 2. LAXS data from oriented PSM. A. After overnight equilibration at 3 °C and B. at 37 °C. D-spacing in A is 60.0 Å, and in B is 63.6 Å.

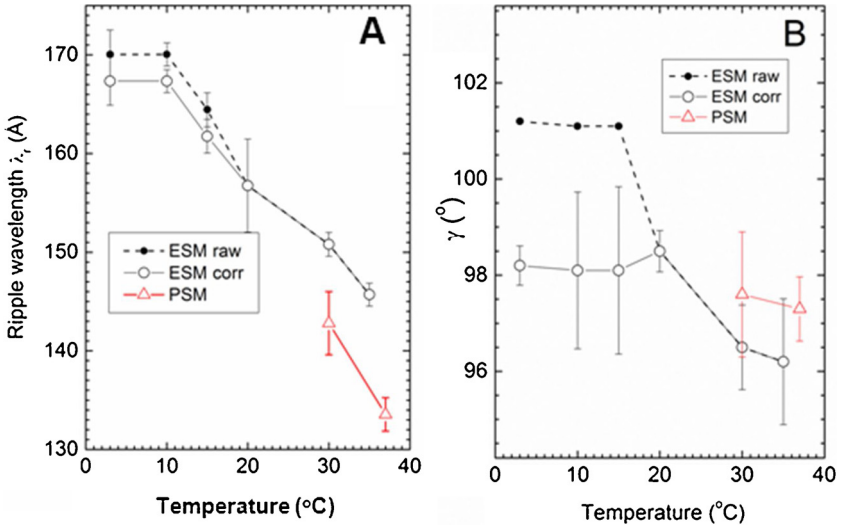

Fig. 4. Temperature dependence of A. λ_r of the ripple phase and B. the γ angle for ESM (open black circles) and PSM (open red triangles). The solid symbols show values before correction for hydration level (*vide infra*).

1996; Yao et al., 1991). Furthermore, the stronger intensity of the negative k peaks compared to the positive k peaks means that the asymmetry for $\gamma > 90^{\circ}$ is as drawn in Fig. 3 (Akabori and Nagle, 2015; Sun et al., 1996b).

Fig. 5 shows wide-angle WAXS scattering for the same PSM sample as in Fig. 2. With the longer exposure time appropriate for the WAXS scattering, Fig. 5A shows LAXS orders h = 1-4 that are overexposed and weak h = 5, 7 and 9 LAXS orders. The WAXS scattering in Fig. 5A looks similar to the WAXS pattern from the $L_{\beta I}$ gel phase in DMPC (Tristram-Nagle et al., 2002), where tilted chains cause the (1,1) peak to be lifted up off the equator near $q_r = 1.4\,Å^{-1}$. Also visible at the same q_r and smaller q_z is a satellite that comes from modulation of the continuous form factor along the (1,1) Bragg rod (Sun et al., 1994). The wide angle scattering in Fig. 5B is consistent with the much higher resolution WAXS from DMPC in the ripple phase (Akabori and Nagle, 2015) suggesting that there is a stronger Bragg rod centered near $q_r = 1.5\,Å^{-1}$ and $q_z \sim 0.3\,Å^{-1}$ and a weaker Bragg rod at smaller q_r and q_z, although such a separation is not visible in Fig. 5B. Figs. S3–S5 for ESM are more suggestive of such a wide angle pattern.

WAXS data shown in Fig. 5A were used to determine the gel phase chain tilt angle for PSM, $\theta_{tilt} = 30.4$, the area/chain perpendicular to the chains, $A_C = 19.2\,Å^2$, and the area/lipid $A_L = 2A_C/\cos\theta_{tilt}$ following (Tristram-Nagle et al., 2002; Tristram-Nagle et al., 1993).

Although data from oriented samples are the more important, unoriented MLV samples are also informative. Fig. 6 shows X-ray scattering from ESM MLVs. In the WAXS regime, a single sharper ring is observed below the transition temperature, indicating chain ordering, and this becomes broad at 50 °C, indicating chain melting. PC lipids have a single sharp WAXS ring in their ripple phase, whereas in their gel phase there are two separate WAXS rings, one sharp and one broader, due to chain tilt. It is important to note that the single WAXS ring below T_M in Fig. 6 does not prove, contrary to what is commonly assumed, that ESM is in a ripple phase. Separation of the two rings in PC lipids is just due to orthorhombic splitting of the hexagonal packing of the chains. A gel phase does not require such splitting, in which case one would also observe a single ring that would be misidentified with a ripple phase.

Several peaks are observed in the LAXS regime in Fig. 6, but these can be satisfactorily indexed as lamellar peaks with no obvious off-specular reflections that would indicate that the sample is in the ripple phase. To further illustrate the difficulty of verifying a ripple phase in unoriented samples, we have taken the oriented data in Fig. 1A and powder averaged it into isotropic rings (Fig. 7); this blurs the relatively weak but clearly separated off-specular peaks in Fig. 1A with the lamellar orders and gives intensity plots similar to the isotropic data in Fig. 6B.

There is one advantage of unoriented MLV samples, which are immersed in excess water and are therefore fully hydrated, over our oriented samples, which are hydrated from the vapor. While it is an advantage to be able to hydrate oriented samples to different D-spacings, it is time consuming to achieve the preferred full hydration. As we have shown previously, D-spacing is extremely sensitive to humidity close to

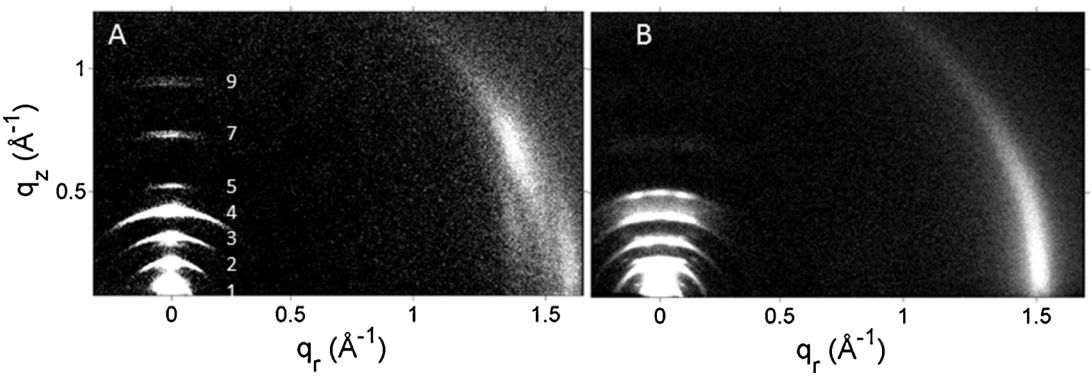

Fig. 5. Wide angle WAXS intensity together with overexposed LAXS for the same sample and temperatures as in Fig. 2. A. PSM at 3 °C, B. PSM at 37 °C. D-spacing in A is 59.2 Å, and in B it is 63.0 Å.

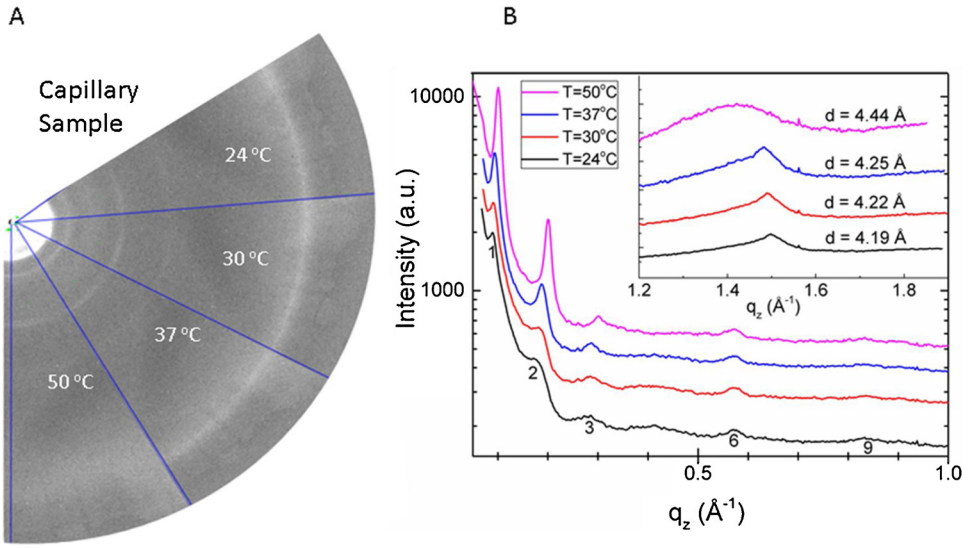

Fig. 6. A. X-ray scattering data from ESM MLVs in a glass capillary collected on a 2D CCD detector at the temperatures indicated. The rings close to the beam (white center) are in the LAXS regime, while the single ring close to the edge of the pie sectors is in the WAXS regime. **B.** Intensity plots of capillary data shown in A. Small black numbers indicate lamellar orders, h = 1,2,3,6,9. Inset: zoomed WAXS region.

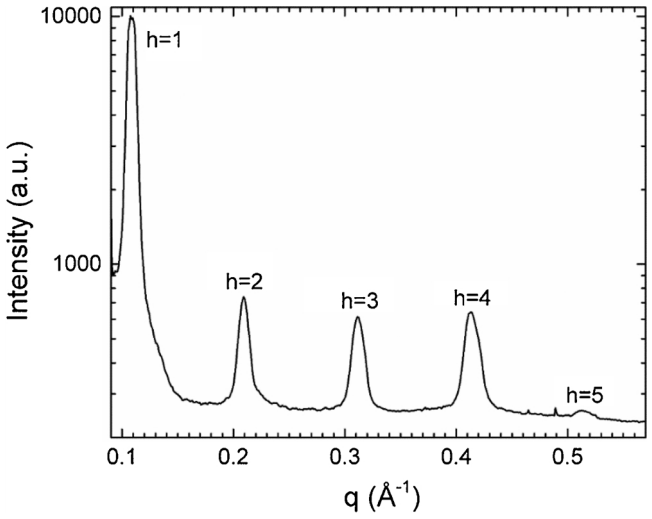

Fig. 7. Powder average of LAXS data shown in Fig. 1A, ESM at 3 °C. As shown, off-specular side peaks are difficult to distinguish from the background scattering between lamellar peaks (numbered). D-spacing is 60.3 Å.

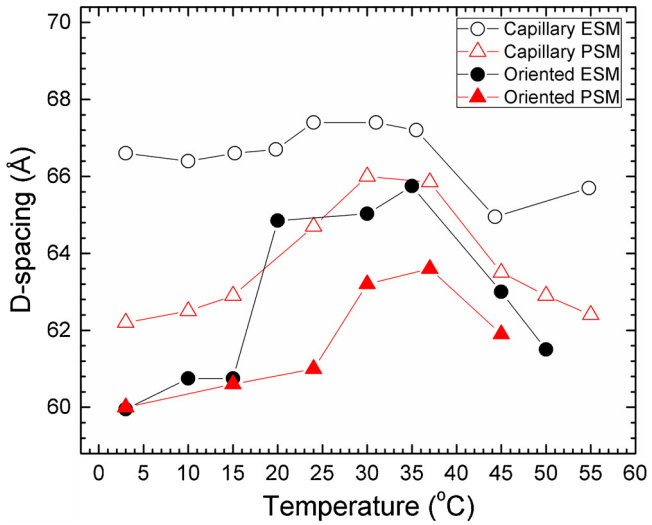

Fig. 8. D-spacings of capillary and oriented samples as a function of temperature (see legend for details).

100% relative humidity (Chu et al., 2005). Fig. 8 compares the actual D-spacings of our oriented samples with those of the fully hydrated MLV samples. Although we did not achieve full hydration for all temperatures in the oriented samples, our experience has been that this amount of dehydration is small enough that the basic properties of fluid and gel phase bilayers are little changed. In Supplementary material, it is shown how our capillary data compare to capillary D-spacings from the literature (Fig. S16).

However, relative humidity affects the values of the ripple phase unit cell parameters as is shown in Fig. 9 for PSM. This impacts the temperature dependence of the raw data in Fig. 4 because those values are affected by both temperature and relative humidity. Fig. 8 shows how much the hydration level differed from full hydration in terms of the D-spacing for our samples at different temperatures. Fig. 9 shows how much λ_r and γ change as a function of D-spacing at the same temperature. Combining these two sets of data allows us to estimate the effect of temperature alone, as is shown by the corrected values in Fig. 4.

Density data yielded a molecular volume for ESM as shown in Fig. 10A. The main phase transition was centered at T_M = 38.3 °C, but it was broad (~4°) as expected for a mixture of chain lengths. No pretransition was observed for ESM. Similar density traces were obtained for PSM, but the absolute molecular volumes are not accurate because the amount of material was much smaller and was not quantitated

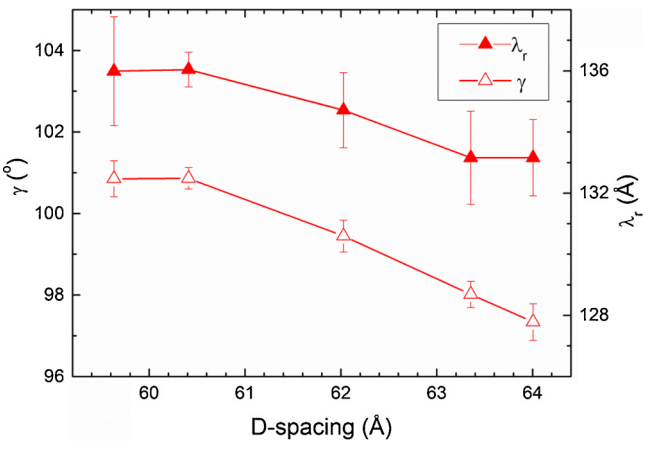

Fig. 9. Effect of hydration level, as indicated by D-spacing, upon unit cell parameters λ_r (solid red triangles, right axis) and γ (open red triangles, left axis). Sample was PSM at 37 °C.

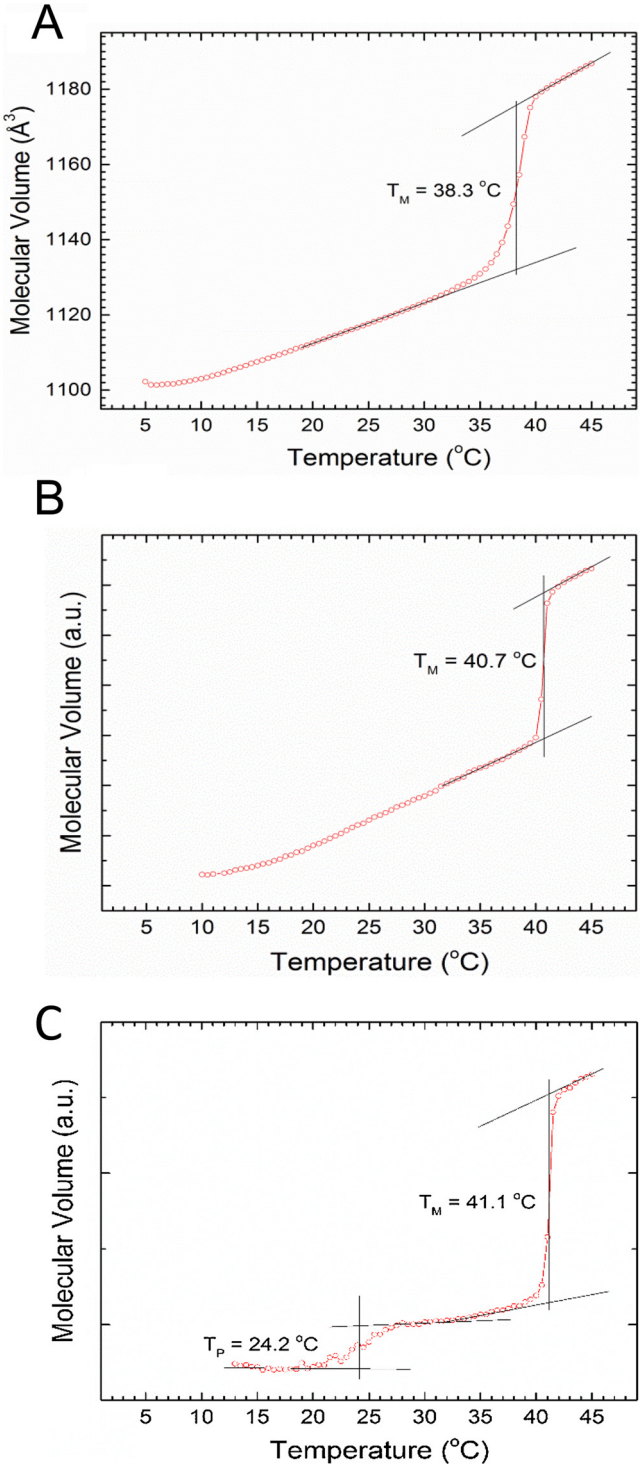

Fig. 10. A. Densitometer scan of ESM immediately after cooling to 3 °C. B. Densitometer scan of PSM immediately after cooling to 3 °C. C. Densitometer scan of PSM after incubating the sample at 3 °C for 4-1/2 days. The T_M was determined as the midpoint of the straight line connecting the extensions of the upper and lower slopes. The heating rate was 12 °C/h.

precisely. The scan in Fig. 10B gave T_M = 40.7 °C for PSM with a smaller width of ~2°, but no pretransition was visible. However, when the sample was held at 3 °C for 4.5 days, a pretransition was readily visible at T_P = 24.2 °C in Fig. 10C, which is a similar value to the DSC literature results for T_P shown in Table S1.

For the fluid phase, the form factors (Fig. S17) that result from diffuse LAXS (Figs. S8 and S15) and the measured volume data were

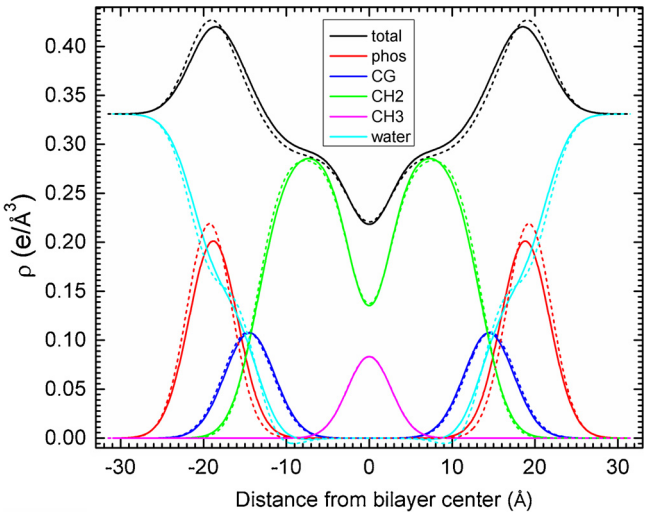

Fig. 11. Electron density profiles of PSM (solid lines) and ESM (dashed lines) in the fluid phase at 45 °C. Bilayer components are: total (black), phosphocholine headgroup (red), glycerol backbone linkage (blue), CH2 groups (green), terminal CH3 groups (magenta) and water (cyan). (For interpretation of the references to colour in this figure legend, the reader is referred to the web version of this article.)

used to construct electron density profiles (Fig. 11) which were then used to obtain A_L at 45 °C by fitting to a model of the electron density of a bilayer (Scattering Density Profile program) (Kučerka et al., 2008). One input into the SDP program is the headgroup volume with the volume ratio of the two headgroup components (phosphocholine and sphingosine linkage). To estimate these, we subtracted the hydrocarbon chain volume from the total lipid volume (see 4.5); the sphingosine linkage volume was obtained by subtracting the phosphocholine volume from the total headgroup volume (Armen et al., 1998).

4. Discussion

4.1. Identification of phases

The most important result from this work is the difference in phase behavior between ESM and PSM at $T < T_M$. We clearly find that the ripple phase in ESM is the stable phase below the main transition at least down to 3 °C. Our result that there is no phase transition below the main transition at T_M agrees with many previous investigations that have reported only a single transition in ESM at 36–39.5 °C by differential scanning calorimetry (Calhoun and Shipley, 1979; Chien et al., 1991; Filippov et al., 2006; Garcia-Arribas et al., 2016; Jimenez-Rojo et al., 2014; Mannock et al., 2003; Mckeone et al., 1986), scanning densitometry (Epand and Epand, 1980), fluorescence spectroscopy (Rujanavech et al., 1986), ^{2}H NMR spectroscopy (Steinbauer et al., 2003) and FTIR spectroscopy (Anderle and Mendelsohn, 1986; Arsov and Quaroni, 2008; Veiga et al., 2001). (Additional DSC literature results are summarized in Table S1). However, in all of these studies, the transition at T_M was interpreted as a gel-to-fluid transition, whereas our results clearly identify the main transition as a ripple-to-fluid transition. Our result agrees with previous X-ray studies that have reported a ripple phase for ESM. The SAXS data of (Chemin et al., 2008) showed weak (0,1) and (1,1) ripple reflections. Using X-ray diffraction, (Shaw et al., 2012) found that the SAXS pattern below T_M in ESM showed a number of broad peaks which could not be resolved from each other. These peaks fit within the same envelope as the ripple phase peaks of bovine brain sphingomyelin which they were able to resolve, so they concluded that ESM was also likely to be in a ripple phase below T_M. A third X-ray investigation reported that after prolonged equilibration at 20 °C, bilayers of ESM formed a ripple structure with a somewhat

Table 1
Elastic and structural results for gel and fluid phases.

Sample	$K_C \times 10^{-20}$ (J)[a]	S_{xray}	A_L (Å^2)	Tilt Angle θ_{tilt} (°)	D_B (Å)
PSM (fluid, 45 °C)	8.3 ± 0.1	0.54 ± 0.02	64 ± 2	–	36.6 ± 1.2
ESM (fluid, 45 °C)	6.7 ± 0.4	0.48 ± 0.02	64 ± 2	–	37.1 ± 1.2
DPPC (fluid, 50 °C)[b]	6.7 ± 0.7	0.41 ± 0.03	64 ± 1[b]	–	38.5 ± 0.5[b]
			63 ± 1[c]		39 ± 0.5[c]
PSM (gel, 3 °C)	–	–	44.5 ± 0.5	30.4 ± 0.6	49.4 ± 0.3
DPPC (gel, 3 °C)[d]	–	–	47.0 ± 0.3	34.0 ± 0.4	48.0 ± 0.2

[a] Results without including a tilt degree of freedom (Nagle, 2017).
[b] (Guler et al., 2009).
[c] (Kučerka et al., 2008).
[d] (Sun et al., 1996a).

smaller periodicity of 125 Å that was obtained from the (0,1) in-plane reflection (Quinn and Wolf, 2009). Based on this peak and on their WAXS results, the authors suggested that at 20 °C ESM showed a phase coexistence of a ripple phase with an interdigitated phase, but it appears that they misinterpreted the higher order ripple peaks. Unlike these previous X-ray works which studied isotropic MLV samples, our oriented samples much more clearly show a rippled phase that is stable from 35 down to 3 °C. This is because oriented samples have clear separations between lamellar and off-specular peaks (Hentschel and Rustichelli, 1991), that are easily measured using a two-dimensional detector.

In contrast to ESM, in PSM the ripple phase is only stable down to about 24 °C and below that the stable phase is a flat gel phase. Previous structural studies (Calhoun and Shipley, 1979; Maulik and Shipley, 1996) found no evidence for a ripple phase in PSM. Some calorimetric studies (Maulik and Shipley, 1996) did not observe a pre-transition in PSM and concluded that PSM is in the gel phase below T_M. Other calorimetric studies reported a pre-transition (Barenholz and Shinitzky, 1976; Calhoun and Shipley, 1979), and those are consistent with our PSM structural results. It has been suggested that this difference in results may be due to the synthesis of PSM yielding a fraction in the L-threo form instead of the D-erythro form (Ramstedt and Slotte, 1999; Venable et al., 2014). In contrast, the Avanti supplied lipid is greater than 98% D-erythro PSM. In any case, we believe that we have now established the PSM phase behavior and that it differs from ESM.

What could be the origin of the stability of the ripple phase in ESM? Recall that the fatty acid composition of Avanti Polar Lipid ESM is 86% 16:0, 6% 18:0, 3% 22:0, 3% 24:0 and 2% unknown. We suggest that it is the presence of a small percentage of longer chain length lipids (18, 22 and 24 carbons) that stabilize the ripple phase in ESM, perhaps by locating in the major arm (M), since the major arm has been shown to be thicker than the minor arm (m), at least in DMPC (Akabori and Nagle, 2015; Sun et al., 1996b). Adding longer chain lipids to the M arm would then increase the disparity between the M and m arms, which would have the tendency to stabilize the ripple phase in ESM to lower temperature. Future experiments on well-defined mixtures could test this suggestion.

4.2. Ripple phase wavelength λ_r

The temperature change is the primary modulator of the ripple structure in our study. As shown in Fig. 4A for ESM, the ripple wavelength λ_r decreases from ~170 to 145 Å over a 32 ° increase. This result is in the same direction, but not as dramatic, as that observed using X-ray diffraction for DMPC, where the ripple repeat decreased from 135 to 120 Å when the temperature increased from 15.2 to 20 °C (Matuoka et al., 1994).

4.3. Ripple phase gamma angle γ

Hydration is the primary modulator of the stacking angle γ which is an indicator of the asymmetry of ripples (Lubensky and Mackintosh, 1993). Asymmetric ripples are defined by the length of the M arm being different from the length of the m arm. Then, interbilayer interactions establish different thickness of the water layers between adjacent bilayers and the stacking of adjacent unit cells may be shifted along the x axis as well as along the z axis, thereby resulting in a value of γ not necessarily equal to 90°. In contrast, if the ripples were symmetric, γ would necessarily be 90°. In *l*-DPPC and *dl*-DPPC (Katsaras et al., 2000) as well as in DMPC (Wack and Webb, 1989) γ decreases as a function of increasing D-spacing. In *l*-DPPC, γ decreased from ~98° at 64 Å to ~90° at 68 Å, and then decreased further to 85° at 73 Å lamellar D-spacing (Katsaras et al., 2000). In ESM, we find that γ > 90° at our largest D-spacings close to T_M, although these D-spacings are not as large as those for *l*-DPPC. In PSM γ decreases from 101 to 98° at lamellar D from 59.5 to 64 Å (Fig. 9). For the same level of hydration, Fig. 4B indicates little effect of temperature on γ.

4.4. Gel and fluid phase properties

Results for PSM and ESM are summarized in Table 1, including bending modulus K_C and the order parameter S_{xray} (Mills et al., 2008) in the fluid phase, area/lipid A_L, bilayer thickness ($D_B = V_L/A_L$) and tilt angle θ_{tilt} in the gel phase. As shown, there was little difference in fluid phase structure between ESM and PSM, although PSM was stiffer than ESM and somewhat more ordered as determined by S_{xray}. Literature results for DPPC are shown for comparison. Except for the considerably smaller value of S_{xray}, which agrees with NMR(S_{CD}) result of (Mehnert et al., 2006), differences are small. Further comparison of these results with X-ray and NMR studies from the literature can be found in Tables S2 and S3.

Results for the gel phase of PSM are also compared in Table 1 to results for DPPC extrapolated to 3 °C. Not shown in Table 1 are values for the area/chain A_C perpendicular to the chains. That value is 19.2 ± 0.2 Å^2 for PSM and for DPPC it is 19.5 ± 0.2 Å^2 (Sun et al., 1996a). This indicates a slightly tighter packing of PSM than DPPC. The other primary difference is the smaller tilt angle in PSM. Those two differences make the area/lipid of PSM noticeably smaller through the relation $A_L = 2A_C/\cos\theta_{tilt}$.

4.5. Contact with MD simulations

Simulations are generally very poor for ripple phases and even problematic for gel phases. However, it is appropriate to compare to MD simulations of sphingomyelins in the fluid phase. One point of contact we can make presently is with our most accurately obtained volume of 1187 ± 1 Å^3 at 45 °C for ESM in the fluid phase. To compare to simulations of PSM at 50 °C, we added 6 Å^3 for thermal expansion using (Nagle and Wilkinson, 1978) and subtracted 27 Å^3 per extra methylene to account for the longer chains in the ESM mixture to obtain 1178 Å^3. Lipid volumes from GROMACS MD simulations of PSM at 50 °C yielded 1168 ± 12 Å^3 (Metcalf and Pandit, 2012) and

1180 ± 10 Å^3 (Niemela et al., 2004). Another point of contact is our A_L of 64 Å^2 for both ESM and PSM. Our area in Table 1 is significantly larger than the average 54 ± 3 Å^2 obtained in several MD simulations (Venable et al., 2014) (and references therein), which suggests that the SM force fields might have to be re-evaluated.

4.6. General comment

Our results address the question of whether the less expensive ESM mixture is likely to be a suitable replacement for the more specific PSM lipid in raft studies that assume that ESM is a single component or when comparing simulations that use PSM to compare to experimental data obtained using ESM. Our result that the lipid areas are essentially the same is encouraging that such replacements can be used in the fluid phase, which is where simulations are most reliable. However, for phase behavior, our results show different propensities to form ripple versus gel phases. While ripple phases are unlikely to form in ternary mixtures, the different propensity to form ripple phases shows that PSM and ESM have different interactions that could affect the stability of liquid ordered phases in lipid raft mixtures, depending on which lipid is used. However, this difference occurs only for temperatures substantially below the main transition temperature, which is itself different by a few degrees between ESM and PSM. Probably, these differences would only be significant for the most careful studies of phase behavior.

Author contributions

Felix Goñi and Stephanie Tristram-Nagle conceived this project, which is part of a larger study of SM mixtures. John Nagle and Stephanie Tristram-Nagle instructed Emilio González-Ramírez in X-ray and densitometer data collection and analysis. Emilio González-Ramírez and Zoran Arsov collected and analyzed X-ray and densitometer data. Zoran Arsov, Stephanie Tristram-Nagle and John Nagle wrote the paper. John Nagle takes responsibility for the integrity of the work as a whole, from inception to finished article.

Acknowledgements

We thank Dr. Steve Burgess at Avanti Polar Lipids for providing detailed information regarding the purity of PSM. Z.A. acknowledges financial support by the Slovenian Research Agency (research program No. P1-0060) and the Fulbright Visiting Scholar Program. E.J.G.-R. acknowledges the University of the Basque Country for a pre-doctoral grant. F.M.G. acknowledges the Spanish Ministry of Economy (BFU 2015-66306-P) and the Basque Government (IT-849-13). S.T.-N. acknowledges financial support from the Samuel and Emma Winters Foundation.

Appendix A. Supplementary data

Supplementary data associated with this article can be found, in the online version, at https://doi.org/10.1016/j.chemphyslip.2018.03.003.

References

Akabori, K., Nagle, J.F., 2015. Structure of the DMPC lipid bilayer ripple phase. Soft Matter 11, 918–926.
Anderle, G., Mendelsohn, R., 1986. Fourier-transform infrared studies of CaATPase phospholipid interaction − survey of lipid classes. Biochemistry-Us 25, 2174–2179.
Armen, R.S., Uitto, O.D., Feller, S.E., 1998. Phospholipid component volumes: determination and application to bilayer structure calculations. Biophys. J . 75, 734–744.
Arsov, Z., Quaroni, L., 2008. Detection of lipid phase coexistence and lipid interactions in sphingomyelin/cholesterol membranes by ATR-FTIR spectroscopy. Biochim. Biophys. Acta 1778, 880–889.
Barenholz, Y., Shinitzky, M., 1976. Effect of sphingomyelin level on membrane dynamics. Israel J. Med. Sci. 12, 1362–1363.
Barenholz, Y., Suurkuusk, J., Mountcastle, D., Thompson, T.E., Biltonen, R.L., 1976. A calorimetric study of thermotropic behavior of aqueous dispersions of natural and synthetic sphingomyelins. Biochemistry-Us 15, 2441–2447.
Calhoun, W.I., Shipley, G.G., 1979. Fatty-acid composition and thermal-behavior of natural sphingomyelins. Biochim. Biophys. Acta 555, 436–441.
Chemin, C., Bourgaux, C., Pean, J.M., Pabst, G., Wuthrich, P., Couvreur, P., Ollivon, M., 2008. Consequences of ions and pH on the supramolecular organization of sphingomyelin and sphingomyelin/cholesterol bilayers. Chem. Phys. Lipids 153, 119–129.
Chien, K.Y., Huang, W.N., Jean, J.H., Wu, W.G., 1991. Fusion of sphingomyelin vesicles induced by proteins from Taiwan cobra (Naja–Naja Atra) venom − Interactions of zwitterionic phospholipids with cardiotoxin analogs. J. Biol. Chem. 266, 3252–3259.
Chu, N., Kučerka, N., Liu, Y.F., Tristram-Nagle, S., Nagle, J.F., 2005. Anomalous swelling of lipid bilayer stacks is caused by softening of the bending modulus. Phys. Rev. E 71, 041904.
de Almeida, R.F.M., Fedorov, A., Prieto, M., 2003. Sphingomyelin/phosphatidylcholine/cholesterol phase diagram: boundaries and composition of lipid rafts. Biophys. J. 85, 2406–2416.
van Meer, G., Voelker, D.R., Feigenson, G.W., 2008. Membrane lipids: where they are and how they behave. Nat. Rev. Mol. Cell Biol. 9, 112–124.
Epand, R.M., Epand, R.F., 1980. Studies of thermotropic phospholipid phase-transitions using scanning densitometry. Chem. Phys. Lipids 27, 139–150.
Filippov, A., Oradd, G., Lindblom, G., 2006. Sphingomyelin structure influences the lateral diffusion and raft formation in lipid bilayers. Biophys. J . 90, 2086–2092.
Garcia-Arribas, A.B., Axpe, E., Mujika, J.I., Merida, D., Busto, J.V., Sot, J., Alonso, A., Lopez, X., Garcia, J.A., Ugalde, J.M., Plazaola, F., Goni, F.M., 2016. Cholesterol-ceramide interactions in phospholipid and sphingolipid bilayers as observed by positron annihilation lifetime spectroscopy and molecular dynamics simulations. Langmuir: ACS J. Surf. Colloids 32, 5434–5444.
Goni, F.M., Alonso, A., 2006. Biophysics of sphingolipids I. Membrane properties of sphingosine: ceramides and other simple sphingolipids. Biochim. Biophys. Acta 1758, 1902–1921.
Guler, S.D., Ghosh, D.D., Pan, J., Mathai, J.C., Zeidel, M.L., Nagle, J.F., Tristram-Nagle, S., 2009. Effects of ether vs ester linkage on lipid bilayer structure and water permeability. Chem. Phys. Lipids 160, 33–44.
Hentschel, M.P., Rustichelli, F., 1991. Structure of the ripple phase P-beta' in hydrated phosphatidylcholine multimembranes. Phys. Rev. Lett. 66, 903–906.
Jimenez-Rojo, N., Garcia-Arribas, A.B., Sot, J., Alonso, A., Goni, F.M., 2014. Lipid bilayers containing sphingomyelins and ceramides of varying N-acyl lengths: a glimpse into sphingolipid complexity. Biochim. Biophys. Acta 1838, 456–464.
Katsaras, J., Tristram-Nagle, S., Liu, Y., Headrick, R.L., Fontes, E., Mason, P.C., Nagle, J.F., 2000. Clarification of the ripple phase of lecithin bilayers using fully hydrated, aligned samples. Phys. Rev. E 61, 5668–5677.
Kučerka, N., Nagle, J.F., Sachs, J.N., Feller, S.E., Pencer, J., Jackson, A., Katsaras, J., 2008. Lipid bilayer structure determined by the simultaneous analysis of neutron and X-ray scattering data. Biophys. J. 95, 2356–2367.
Kučerka, N., Liu, Y.F., Chu, N.J., Petrache, H.I., Tristram-Nagle, S.T., Nagle, J.F., 2005. Structure of fully hydrated fluid phase DMPC and DLPC lipid bilayers using X-ray scattering from oriented multilamellar arrays and from unilamellar vesicles. Biophys. J . 88, 2626–2637.
Lubensky, T.C., Mackintosh, F.C., 1993. Theory of ripple phases of lipid bilayers. Phys. Rev. Lett. 71, 1565–1568.
Mannock, D.A., McIntosh, T.J., Jiang, X., Covey, D.F., McElhaney, R.N., 2003. Effects of natural and enantiomeric cholesterol on the thermotropic phase behavior and structure of egg sphingomyelin bilayer membranes. Biophys. J . 84, 1038–1046.
Mason, P.C., Gaulin, B.D., Epand, R.M., Wignall, G.D., Lin, J.S., 1999. Small-angle scattering studies of the fully hydrated phospholipid DPPC. Phys. Rev. E 59, 921–928.
Matuoka, S., Kato, S., Hatta, I., 1994. Temperature-change of the ripple structure in fully hydrated dimyristoylphosphatidylcholine cholesterol multibilayers. Biophys. J . 67, 728–736.
Maulik, P.R., Shipley, G.G., 1996. N-palmitoyl sphingomyelin bilayers: structure and interactions with cholesterol and dipalmitoylphosphatidylcholine. Biochemistry-Us 35, 8025–8034.
Mckeone, B.J., Pownall, H.J., Massey, J.B., 1986. Ether phosphatidylcholines − comparison of miscibility with ester phosphatidylcholines and sphingomyelin, vesicle fusion, and association with apolipoprotein-a-I. Biochemistry-Us 25, 7711–7716.
Mehnert, T., Jacob, K., Bittman, R., Beyer, K., 2006. Structure and lipid interaction of N-palmitoylsphingomyelin in bilayer membranes as revealed by H-2-NMR spectroscopy. Biophys. J . 90, 939–946.
Metcalf, R., Pandit, S.A., 2012. Mixing properties of sphingomyelin ceramide bilayers: a simulation study. J. Phys. Chem. B 116, 4500–4509.
Mills, T.T., Toombes, G.E.S., Tristram-Nagle, S., Smilgies, D.M., Feigenson, G.W., Nagle, J.F., 2008. Order parameters and areas in fluid-phase oriented lipid membranes using wide angle x-ray scattering. Biophys. J . 95, 669–681.
Nagle, J.F., Wilkinson, D.A., 1978. Lecithin bilayers: density measurement and molecular interactions. Biophys. J . 23, 159–175.
Nagle, J.F., Akabori, K., Treece, B.W., Tristram-Nagle, S., 2016. Determination of mosaicity in oriented stacks of lipid bilayers. Soft Matter 12, 1884–1891.
Nagle, J.F., 2017. Experimentally determined tilt and bending moduli of single-component lipid bilayers. Chem. Phys. Lipids 205, 18–24.
Niemela, P., Hyvonen, M.T., Vattulainen, I., 2004. Structure and dynamics of sphingomyelin bilayer: insight gained through systematic comparison to phosphatidylcholine. Biophys. J. 87, 2976–2989.
Quinn, P.J., Wolf, C., 2009. Thermotropic and structural evaluation of the interaction of natural sphingomyelins with cholesterol. Biochim. Biophys. Acta 1788, 1877–1889.
Ramstedt, B., Slotte, J.P., 1999. Comparison of the biophysical properties of racemic and d-erythro-N-acyl sphingomyelins. Biophys. J. 77, 1498–1506.
Ramstedt, B., Slotte, J.P., 2002. Membrane properties of sphingomyelins. FEBS Lett. 531, 33–37.

Ramstedt, B., Leppimäki, P., Axberg, M., Slotte, J.P., 1999. Analysis of natural and synthetic sphingomyelins using high-performance thin-layer chromatography. Eur. J. Biochem. 266, 997–1002.
Rappolt, M., Rapp, G., 1996. Structure of the stable and metastable ripple phase of dipalmitoylphosphatidylcholine. Eur. Biophys. J. Biophys. 24, 381–386.
Rujanavech, C., Henderson, P.A., Silbert, D.F., 1986. Influence of sterol structure on phospholipid phase-behavior as detected by parinaric acid fluorescence spectroscopy. J. Biol. Chem. 261, 7204–7214.
Shaw, K.P., Brooks, N.J., Clarke, J.A., Ces, O., Seddon, J.M., Law, R.V., 2012. Pressure-temperature phase behaviour of natural sphingomyelin extracts. Soft Matter 8, 1070–1078.
Slotte, J.P., 2013. Molecular properties of various structurally defined sphingomyelins – correlation of structure with function. Prog. Lipid Res. 52, 206–219.
Slotte, J.P., 2016. The importance of hydrogen bonding in sphingomyelin's membrane interactions with co-lipids. Biochim. Biophys. Acta 1858, 304–310.
Steinbauer, B., Mehnert, T., Beyer, K., 2003. Hydration and lateral organization in phospholipid bilayers containing sphingomyelin: a H-2-NMR study. Biophys. J. 85, 1013–1024.
Sun, W.J., Suter, R.M., Knewtson, M.A., Worthington, C.R., Tristram-Nagle, S., Zhang, R., Nagle, J.F., 1994. Order and disorder in fully hydrated unoriented bilayers of gel phase dppc. Phys. Rev. E. 49, 4665–4676.
Sun, W.J., Tristram-Nagle, S., Suter, R.M., Nagle, J.F., 1996a. Structure of gel phase saturated lecithin bilayers: temperature and chain length dependence. Biophys. J. 71, 885–891.
Sun, W.J., Tristram-Nagle, S., Suter, R.M., Nagle, J.F., 1996b. Structure of the ripple phase in lecithin bilayers. Proc. Natl. Acad. Sci. U. S. A. 93, 7008–7012.
Tristram-Nagle, S., Zhang, R., Suter, R.M., Worthington, C.R., Sun, W.J., Nagle, J.F., 1993. Measurement of chain tilt angle in fully hydrated bilayers of gel phase lecithins. Biophys. J. 64, 1097–1109.
Tristram-Nagle, S., Liu, Y.F., Legleiter, J., Nagle, J.F., 2002. Structure of gel phase DMPC determined by X-ray diffraction. Biophys. J. 83, 3324–3335.
Tristram-Nagle, S., 2007. Preparation of Oriented, Fully Hydrated Lipid Samples for Structure Determination Using X-ray Scattering. Humana Press, Totowa, NJ.
Veiga, M.P., Arrondo, J.L.R., Goñi, F.M., Alonso, A., Marsh, D., 2001. Interaction of cholesterol with sphingomyelin in mixed membranes containing phosphatidylcholine, studied by spin-label ESR and IR spectroscopies. A possible stabilization of gel-phase sphingolipid domains by cholesterol. Biochemistry-Us 40, 2614–2622.
Venable, R.M., Sodt, A.J., Rogaski, B., Rui, H., Hatcher, E., MacKerell, A.D., Pastor, R.W., Klauda, J.B., 2014. CHARMM all-atom additive force field for sphingomyelin: elucidation of hydrogen bonding and of positive curvature. Biophys. J. 107, 134–145.
Wack, D.C., Webb, W.W., 1989. Synchrotron X-ray study of the modulated lamellar phase P-beta' in the lecithin-water system. Phys. Rev. A 40, 2712–2730.
Yao, H., Matuoka, S., Tenchov, B., Hatta, I., 1991. Metastable ripple phase of fully hydrated dipalmitoylphosphatidylcholine as studied by small-angle X-ray-scattering. Biophys. J. 59, 252–255.